Soft Matter

Cite this: DOI: 10.1039/c1sm05668a

www.rsc.org/softmatter

PAPER

Tailoring and probing particle–polymer interactions in PMMA/silica nanocomposites†

M. Qu,[a] J. S. Meth,[b] G. S. Blackman,[b] G. M. Cohen,[b] K. G. Sharp[b] and K. J. Van Vliet*[a]

Received 14th April 2011, Accepted 7th June 2011
DOI: 10.1039/c1sm05668a

The unique physical and mechanical properties of polymer nanocomposites have been attributed to the interfacial interactions between the organic matrix and nanoscale particles. We demonstrate the potential to tune this interaction between poly(methyl methacrylate) (PMMA) and silica nanoparticles, as a function of either nanosilica surface chemistry or polymer reactivity. Functionalized nanosilica was mechanically deposited on the surface of PMMA films, and the system then heated above the polymer glass transition temperature. Rates and extents of nanoparticle sink-in were quantified by timelapse atomic force microscopy-based imaging, showing that the strength of particle–matrix interactions was predicted directly by polymer–particle interaction energies. Nanocomposite films created *via* this approach exhibited significantly enhanced elastic moduli and scratch resistance. This direct quantification of mechanical optimization *via* nanoparticle–polymer interfacial chemistry enables new approaches to rapidly tune nanocomposite performance.

1. Introduction

Composite materials comprising polymer matrices and nanoscale inorganic phases have the potential to exhibit enhanced physical and mechanical properties. In particular, polymer–particle nanocomposites (PPNCs) of less than 20 vol% nanoparticles can show significantly altered fracture toughness,[1–3] elastic moduli[4–7] and glass transition temperatures.[2,6–9] Much progress has been achieved[1–14] in developing PPNCs with high particle dispersion and in characterizing the properties of such bulk composites. However, both mechanical and thermal characterization of these PPNCs has highlighted inconsistent trends that vary among polymers and particle types.[15–18] Thus, it has remained challenging to predict *a priori* whether macroscopic mechanical and thermal properties will increase or decrease for a given PPNC. Several researchers have hypothesized that these varied effects may be due to interaction at the interface region between the polymer and filler particles.[10–14] This polymeric interphase is considered to surround the particle inclusions, and exhibit a degree of molecular confinement or perturbation that gives rise to properties differing from the polymer bulk.[10–12,19] The thickness of this interphase is predicted to be on the order of nanometres, as inferred from both experiments[20–22] and models.[19,23] Thus, polymer–particle interaction at the interface becomes appreciable for even low volume fractions of nanoscale particles.[24] However, despite intensive study and the potential to tune PPNC properties through such understanding, there is little direct evidence demonstrating the existence of this nanoscale interphase. Moreover, there exist few, direct experimental methods suitable to quantify the polymer–nanoparticle interaction at the interface.[51]

Here, we explore the potential to characterize and predict the particle–polymer interactions at this interfacial region. We consider a novel approach to directly quantify the speed and extent of these interactions in PPNCs, enabling rapid comparison and rational tuning of such nanocomposites. We adopt a model system, for which the properties of the poly(methyl methacrylate) (PMMA) matrix and the surface-functionalized silicon dioxide nanoparticles are varied independently. We show that these interactions can be compared directly *via in situ*, timelapsed atomic force microscopy (AFM) imaging at elevated temperatures. Through these approaches, we thus identify the strongest polymer–nanoparticle interactions among these PMMA/nanosilica systems, and show that the stiffness and scratch resistance of such nanocomposite materials is enhanced significantly.

2. Experimental

2.1 Materials and sample preparation

Two polymer matrices were considered: PMMA (M_w = 247.5 kg mol^{-1} and PDI = 1.1, Polysciences) and PMMA/MAA (containing 1.4 wt% methacrylic acid, M_w = 40 kg mol^{-1}, Elvacite™ 2008, Lucite International, Inc). The glass transition temperatures T_g of bulk PMMA and PMMA/MAA were T_g = 132 °C and 117 °C, respectively, as measured *via* differential scanning

[a]*Department of Materials Science & Engineering, Massachusetts Institute of Technology, Cambridge, MA, 02139, USA. E-mail: krystyn@mit.edu*
[b]*DuPont Nanocomposite Technologies, Central Research & Development, DuPont Co., Wilmington, DE, 19808, USA*
† Electronic supplementary information (ESI) available. See DOI: 10.1039/c1sm05668a

calorimetry (Q2000, TA Instruments). Nanosilica particles with two surface chemistries were selected to probe the particle–polymer interaction: methyl (–CH_3), and amine (–NH_2). Trimethyl silyl functionalized colloidal silica nanoparticles were obtained commercially (Nissan Chemical Co., Organosilicasol™ MEK-ST-MS, radius $r = 9$–12 nm). Amine functionalized silica nanoparticles were prepared by reacting aminophenyl silane with the native hydroxyl groups on colloidal silica nanoparticles (Nissan Chemical Co.) of nominal particle radius $r = 10$ nm with the following procedure: a 25.0 g portion of a 30 wt % colloidal SiO_2 in isopropanol was added to a 250 mL, 3-neck round-bottomed flasks, and diluted with 50.0 g of isopropanol. To the flask, a stirring bar was added and a water-cooled condenser was attached with a drying tube atop it. Rapid stirring was begun at room temperature. With a syringe, 0.64 g of *p*-aminophenyltrimethoxysilane was added at room temperature to the flask. The mixture was heated during the daytime only, purely as a safety precaution, holding it at reflux for a total of 20 h over a 3 day period, and then cooled to room temperature. Unlike reactions with some other aminosilanes, this reaction did not cause the silica to gel. The estimated number of native hydroxyl (–OH) groups on the initial particles was approximately six native hydroxyl groups per nm^2 of silica surface area.[25] The theoretical amount of added aminophenyl silane corresponded to 1.61 molecules/nm^2 of surface area, which is about 27% of the available native hydroxyl groups on this surface. Nitrogen microanalysis (Micro Analysis Inc., Wilmington, DE) was used to estimate the graft density of the amine functional groups on these functionalized nanosilica particles, indicating that approximately 42% of the amine groups was ultimately functionalized onto the particles.

To quantify the extent and rate of nanosilica sink-in, samples were prepared using the 'strike method' developed specifically for this study. Polymer thin films were spin coated onto a silicon wafer. A portion of the aminosilane-modified colloid was diluted to 1.0 wt % SiO_2 (w/w) by stirring 0.5 g of this suspension with 4.5 g of isopropanol. A portion was dried to determine that the solids concentration was 1.2%. This diluted colloid was placed in a bath sonicator and afterward passed though a 0.2 μm GHP syringe filter; some pure isopropanol was passed through a 0.45μm PTFE syringe-filter. A portion of the particle suspension was further diluted to 0.006 wt% by injecting 130 μL into 20.0 g of well-stirred, syringe-filtered isopropanol. One drop of this particle suspension was placed on the polymer substrate and then sandwiched with a UV ozone-cleaned glass coverslip. After solvent evaporation, the coverslip was removed from the sample surface, with the result that nanoparticles remained dispersed across and attached to the polymer surface. The particles did not sink in or embed into the glassy polymer surfaces as a result of this preparation, and *in situ* AFM imaging was later used to quantify the induced sink-in during heating of these strike-prepared samples.

For mechanical analysis (detailed methods in section 2–4) of PPNCs comprising functionalized silica nanoparticles, thin film or quasi-two-dimensional nanocomposites were realized by heating samples prepared *via* the strike method. Here, samples were heated to achieve equal nanoparticle heights (*i.e.*, same root-mean-square surface roughness and particle height distributions, within experimental error) among all samples. Temperatures and times required for each sample were determined from AFM timelapse imaging at $T > T_g$, and the resulting equivalence of particle height distributions was confirmed *via* direct AFM imaging at room temperature.

2.2 *In situ* AFM imaging

PMMA and PMMA/MAA thin films were strike-deposited with silica nanoparticles to achieve high particle dispersion. To monitor the particle–polymer interaction, these particle-decorated surfaces were heated from room temperature to above T_g ($\Delta T = T - T_g \approx 12$ °C, $T_g = 132$ °C and 117 °C, respectively), during continuous AFM imaging in alternating contact (AC) mode (MFP-3D and PolyHeater™, Asylum Research, Santa Barbara, CA). Height and phase images comprising the same group of as-deposited nanoparticles were acquired with a line-scan rate of 1 Hz, over durations above T_g of up to 17 h duration. The AFM cantilever exhibited a nominal probe radius $r \sim 10$ nm, nominal resonant frequency $f = 70$ kHz, and nominal spring constant $= 2$ N m^{-1} (OMCL AC240TS-W2, Olympus, Tokyo). For each condition, 10–20 nanoparticles were monitored *in situ* over up to 17 h of interaction with each polymer surface. The heights of the particles with respect to the free surface of the polymer were calculated directly *via* height image analysis (SPIP, Image Metrology, Horsholm, Denmark). Fig. 1 is an example of the height images acquired on the same group of particles at different temperatures/annealing time. The sample in this experiment was methyl functionalized silica on PMMA. The height profile of the same particles at different annealing times is also shown (Fig. 1 insets). Extent of particle sink-in was quantified as the average particle diameter among all nanoparticles for a given experimental condition, where the standard deviation reflects the distribution in nanoparticle diameters and initial heights. Velocity of particle sink-in was compared among samples as the slope of the average nanoparticle height *vs.* time response at a specific timepoint (15 min).

2.3 Surface and interaction energies

Surface tension of polymers and functionalized silica surfaces was calculated by measuring the contact angle above T_g of each polymer matrix and silica surface, with the temperatures corresponding to AFM time-lapse imaging experiments. Contact angles θ were measured using the sessile drop technique (VCA2000 goniometer, AST Inc.),[26] for at least five experimental repeats per sample. Pure anhydrous ethylene glycol (99.8%, <0.003% water, Sigma Aldrich) was used as the liquid drop, due to its relatively high boiling point of 197 °C.[27] The ethylene glycol was received and stored under refrigeration in the same brown rubber-sealed glass bottle, to prevent increasing of the water content in this solvent. A syringe needle was used to extract the liquid from the rubber-sealed bottle. A small custom-made plate heater was used to heat the polymer films. For each substrate material, the surface tension was calculated as: [28–30]

$$\gamma_{substrate} = \gamma_{substrate} + \gamma_{droplet}\cos\theta \quad (1)$$

$$\gamma_{interface} = \gamma_{substrate} + \gamma_{droplet} - 2\left(\gamma_{substrate}\gamma_{droplet}\right)^{\frac{1}{2}} \quad (2)$$

Flat silica slides were functionalized with the same functional groups used to modify the silica nanoparticles, invoking the assumption that the surface energy of these flat functionalized

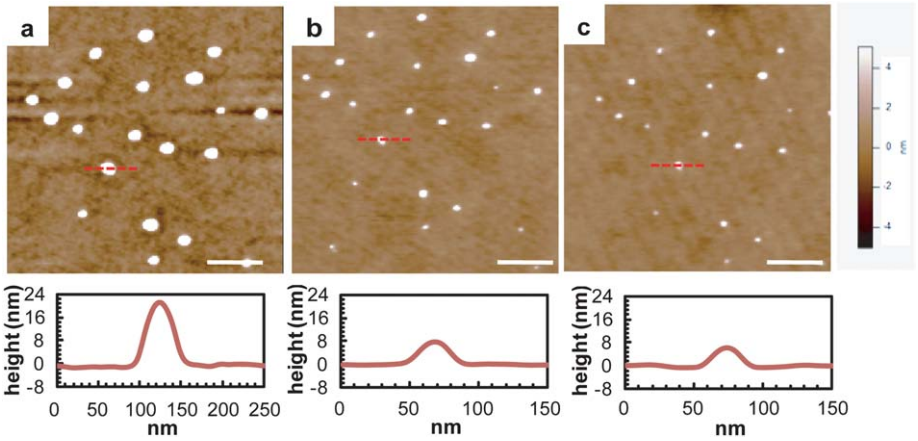

Fig. 1 *In situ* atomic force microscopy imaging, demonstrating methyl functionalized silica nanoparticle height change *vs.* time at constant elevated temperature above T_g of the poly(methyl methacrylate) matrix ($T = 145\,^{\circ}C$). Height traces over a single nanoparticle (red dotted line) in each alternating contact mode topography image are also shown. (a) Room temperature ($t = 0$), (b) $t = 30$ min at elevated temperature, (c) $t = 17$ h at elevated temperature. Scale bar = 200 nm.

silica surfaces is comparable to that of the functionalized silica nanoparticles. To our knowledge, it is not currently possible to rigorously quantify the surface energy of the silica nanoparticles of these diameters, and thus the surface energies measured in this manner are employed as a reasonable surrogate.

2.4 Elastic moduli and scratch resistance of nanocomposites

The elastic moduli E of the thin film PPNCs, prepared as described above, were determined *via* instrumented nanoindentation (TriboIndenter, Hysitron, Inc.). A conospherical diamond indenter of probe radius $R = 10$ μm was used to achieve maximum indentation depths h of ~20 nm at maximum indentation loads P of 600 μN, and thus sample sufficiently large surface areas (~ 1 × 1 μm^2) and volumes to capture the composite response. Twenty replicate indentations were conducted on each sample (N = 20). Loading and unloading times were 10 s, with a 10 s dwell at peak load. Reduced elastic moduli (E_r) were calculated according to Hertzian elastic analysis (eqn (3)),

$$p = \frac{4}{3} E_r R^{\frac{1}{2}} h^{\frac{3}{2}} \quad (3)$$

corrected for finite thickness of the nanocomposite films ($t = 500$ nm) on a stiffer Si substrate as described in Constantinides *et al.*[31] Elastic modulus of the composites E was converted using eqn (4):

$$\frac{1}{E_r} = \frac{1 - \nu^2}{E} + \frac{1 - \nu_i^2}{E_i} \quad (4)$$

assuming E_i and ν_i of the diamond probe to be 1070 GPa and 0.07, respectively, and $\nu = 0.5$ for the composites.

Scratch resistance was quantified *via* scratch testing with the same probe. Fifteen replicate scratch experiments (N = 15) were conducted on each sample. Lateral surface scratches were imposed on pure polymer films and thin film PPNCs, with a maximum normal load of 600 μN and scratch length of 10 μm. Scratch resistance was quantified by analyzing the AFM topographical images, and expressed as the volume/length of the residual scratches. At least eight scratches (N = 8) were analyzed for each sample, with this reduced sample set corresponding to exclusion of scratches in areas that were found upon AFM imaging to include surface debris or otherwise low-quality AFM topographic data for subsequent volumetric analysis.

3. Results and discussion

3.1 Quantifying extent of polymer–nanoparticle interactions

In order to tailor the interaction between particle and polymer matrix, both the silica nanoparticle surface chemistry and the polymer matrix chemistry were varied independently. Two nanosilica surface chemistries were considered: methyl and amine. Two different amorphous polymers were considered: poly (methyl methacyrlate) (PMMA) and PMMA/MAA; methacrylic acid provides potential to strongly interact with amine functional groups. Based on the chemical nature of these interfaces, we anticipated that methyl-terminated nanosilica would exhibit the weakest interaction with the PMMA matrix, while amine-terminated nanosilica would exhibit the strongest interaction with PMMA/MAA.

To quantify the rate and extent of these polymer–nanoparticle interactions, particles were deposited onto pure polymer matrix substrates *via* the strike method (see Experimental), and the system was heated above the glass transition temperature of the polymer matrix ($\Delta T = T_g - T = 13\,^{\circ}C$ for PMMA and $\Delta T = 12\,^{\circ}C$ for PMMA/MAA) within an atomic force microscope. Sequential AC-mode topography images were acquired *in situ* over 17 h at this elevated temperature (Fig. 1), to determine the height of each particle relative to the polymer free surface. Note that these nanoparticles exhibited a distribution of diameters over each 1 μm^2 image comprising ~10–20 silica nanoparticles; this is indicated in terms of the standard deviation (~1 nm) in Fig. 2. The average and range of initial particle height was statistically equivalent among all samples prior to heating. Clearly, the nanoparticles sank into the polymer surface upon heating above the polymer T_g, and the speed and extent of this

interaction varied with interfacial chemistry. Figure 2 shows that methyl functionalized nanosilica sank in less than amine functionalized nanosilica, for both the PMMA and PMMA/MAA substrates (Fig. 2a-b). On the PMMA substrate, the final average above-surface height h_s of methyl functionalized nanosilica was 7.7 ± 0.5 nm, while h_s was 6.8 ± 0.4 nm for the amine functionalized nanosilica (Fig. 2c). Further, Fig. 2c shows that nanoparticles embedded into the PMMA/MAA substrate to a greater extent than into the PMMA substrate. In fact, amine functionalized nanosilica embedded fully within the PMMA/MAA (h_s < 0.5 nm), while methyl functionalized nanosilica exhibited a terminal height of 4.1 ± 0.4 nm after 17 h annealing. Figure 3 illustrates this embedding for amine functionalized nanosilica on PMMA/MAA over 17 h of annealing. Note that by 17 h at this elevated temperature, there were no surface features in the topographic images associated with the amine functionalized nanosilica; the particles were beneath the PMMA/MAA surface. The phase lag image indicated occasional dark punctuate features that we associate with nanoparticles located just beneath the surface, which slightly changes the dynamics of the vibrating AFM cantilever. Together, these data confirmed that, as predicted, the amine functionalized nanosilica interacted more strongly with these PMMA-based polymers than the methyl functionalized nanosilica, and that the strongest nanoparticle–polymer interaction was achieved between the amine functionalized nanosilica and PMMA/MAA matrix. Next we related these dynamic observations of particle–polymer interactions to the underlying thermodynamics and kinetics at this interface.

3.2 Effects of surface energy on nanoparticle–polymer interactions

To further understand the thermodynamic mechanisms promoting these nanoparticle–polymer interactions, surface

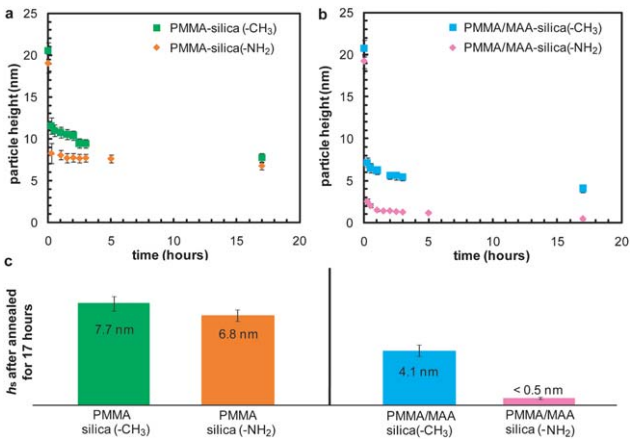

Fig. 2 *In situ* atomic force microscopy imaging at elevated temperature above T_g shows the change in silica nanoparticle height h_s *vs.* time t for poly(methyl methacrylate) or PMMA (T = 145 °C) and for PMMA/methacrylic acid or MAA (T = 129 °C); $\Delta T = T - T_g \sim 12$ °C. (a) PMMA-nanosilica and (b) PMMA/MAA-nanosilica samples prepared *via* the strike method described in the text. (c) Average nanoparticle height h_s protruding above the polymer surface at t = 17 h indicates the difference in extent of nanosilica-polymer interactions as a function of particle and polymer chemistry.

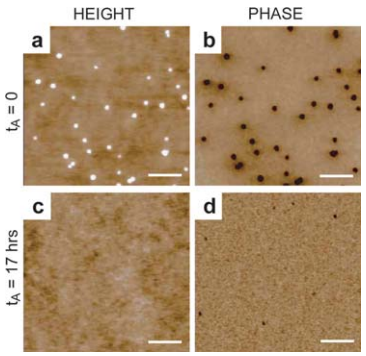

Fig. 3 Atomic force microscopy height and phase images, acquired in alternating contact mode for amine functionalized nanosilica on poly (methyl methacrylate)/methacrylic acid at (a, b) time prior to heating of the sample; and (c, d) 17 *h* after heating of the sample at elevated temperature $T - T_g \sim 12$ °C. Complete embedding of the amine-functionalized nanosilica is obtained within 17 h at this temperature. Scale bar = 200 nm.

tension of both the polymers and the functionalized silica was measured at elevated temperature ($\Delta T \sim 12$ °C) using sessile droplet angle analysis (see Experimental and ESI,† Fig. S1). As summarized in Fig. 4a, PMMA/MAA exhibited a lower surface tension (26.2 ± 0.6 mN m^{-1}) than PMMA (30.4 ± 0.7 mN m^{-1}) at the relevant temperatures. Note that the measured surface tension of PMMA at T = 142 °C was comparable to previous findings at 150 °C (31.2 mN m^{-1}).[32] For the PMMA/MAA copolymer, one may have expected the surface energy to by higher than that of PMMA due to the presence of the acrylic acid groups. However, this expectation should apply only for polymer precipitated from solution, where the acid groups would be near the surface due to interaction with the solvent. When such polymers are heated, and the macromolecular chain mobility increases, the surface will physically rearrange to minimize the surface energy. Therefore, it is reasonable that the surface energies of these two polymers are similar quantitatively. The difference can be attributed to the known molecular weight dependence of the surface energy. Together, these data imply that less thermodynamic work is required for particles to sink into the PMMA/MAA surface than into the PMMA, and is consistent with our experimental observations in Fig. 2. Further, Fig. 4a shows that the amine functionalized silica exhibited a higher surface energy (26.3 ± 0.5 mN m^{-1}) than methyl functionalized silica (18.6 ± 1.0 mN m^{-1}). These measured surface energies of functionalized silica are slightly lower than but still comparable to literature values for amine functionalized and methyl functionalized silica, respectively (36.3 mN m^{-1} and 24.3 mN m^{-1} [33,34]). Note that surface tension of these functionalized particles and polymers is indicated in primary colors in Fig. 4; subsequently, the properties of nanocomposites rendered from pairwise combinations are represented by the blends of those colors.

Kovacs *et al.* proposed an energetic interaction parameter between particles and polymers, based on the assumption that the extent of a particle embedding into a polymer surface at elevated temperature is related to relative surface energies. This parameter can be expressed as:

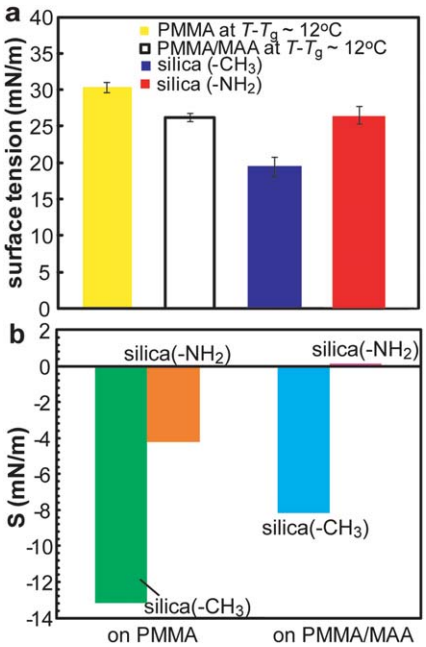

Fig. 4 (a) Surface tension of the polymers and functionalized silica, all measured at elevated temperature of ~140 °C; polymers were characterized at their respective $T - T_g$ ~12 °C. (b) Energetic interaction parameter S computed from these surface tensions, which predicts that functionalized silica will embed within the polymer at elevated temperatures if $S > 0$.

$$S = \gamma_1 - \gamma_{12} - \gamma_2 \quad (5)$$

where γ_1 is the surface tension of the particle material, γ_2 is the surface tension of the polymer measured above the corresponding T_g, and γ_{12} is the interfacial tension between the particle and polymer. Incomplete particle embedding or sink-in is expected if $S < 0$ while complete embedding is expected if $S > 0$.[28,29,35–37] Here, we employ eqn (5) to interpret particle–polymer interactions in polymer nanocomposites. Note that other measures of surface energy-based interactions are also used to estimate the strength of particle–polymer interaction; work of spreading is adopted in the carbon black-rubber composite community.[38–41] In this study, surface tension of planar silica with the same functional groups used to modify the silica nanoparticles were measured as γ_1, invoking the assumption that the surface energy of these flat functionalized silica surfaces is comparable to that of the functionalized silica nanoparticles (see Experimental). Using the same solvent for both the functionalized silica and the polymer surfaces, S was calculated from eqn (5). Fig. 4b shows that $S < 0$ for all particle–polymer composite systems, with the exception of the PMMA/MAA-amine functionalized silica. This finding indicates that complete particle embedding is predicted only for amine functionalized silica in the PMMA/MAA matrix. This thermodynamics-based prediction is well matched by the experimental results in Fig. 2. Thus, surface energy measurements are verified as an efficient method to predict the extent of particle–polymer interactions, which can serve as a guide for chemical modification of both particles and polymer matrices comprising nanocomposites.

3.3 Effects of kinetics on the nanoparticle–polymer interactions

To further understand the kinetics of these interactions, we considered the temporal evolution of the nanoparticle sink-in at the polymer surface. This measurement related to experiment-specific issues such as the extent to which temporal characteristics of the polymer (*e.g.*, viscosity at a specific temperature) influenced this nanoparticle sink-in. Moreover, this rate of nanoparticle–polymer interactions is related to the rate at which nanoparticles can become dispersed within a polymer matrix. Figure 5 shows the average particle sink-in velocity u at $t = 15$ min, termed the initial sink-in velocity; note that more than half of the total particle height change occurred within the initial 15 min at this constant temperature above T_g (see Experimental). Clearly, u was significantly greater for amine functionalized nanosilica on both PMMA and PMMA/MAA, exceeding the velocity of the methyl functionalized nanosilica counterpart by 17% and 33%, respectively.

Further, Fig. 5 shows that nanosilica of identical functionalization sinks in at higher velocities on PMMA/MAA, with u greater by 70% and 50% for amine- and methyl-functionalized nanosilica, respectively. This relative difference between the two polymer types may be attributed to a combination of two effects: first, the lower molecular weight of the PMMA/MAA would manifest as a reduced viscosity above T_g, which reduces the time scale of particle sink-in; second, the chemical functionality of the acrylic acid co-monomer enhances the interaction energy between the particle and polymer and thus increases the energetic driving force for embedding. To estimate the extent to which changes in polymer viscosity may influence particle sink-in velocity, we employed a modified Stokes–Einstein (SE) diffusion equation to account explicitly for polymer viscosity:[28,37]

$$\frac{4}{3}x^3 + x^4 + \frac{x^5}{5} = \frac{tA}{9\pi\eta r^3} \quad (6)$$

Here, t is time at elevated temperature, r is particle radius, η is polymer viscosity, and $x = z/r$, which is the normalized particle sink-in depth z obtained directly from AFM height images. The term A is the Hamaker interaction constant between silica and polymer, where $A = (A_{silica}A_{polymer})^{0.5}$ J $= 5.45 \times 10^{-20}$ J for the material-specific constants ($A_{PMMA} = 3.45 \times 10^{-21}$ J[42] and

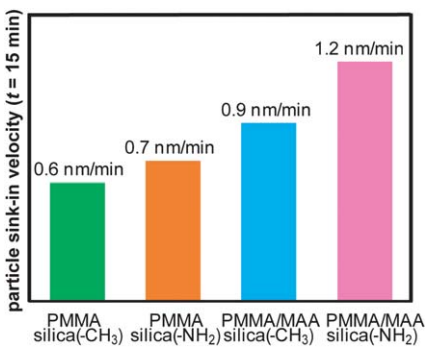

Fig. 5 Average particle sink-in velocity at $t = 15$ min, as determined from *in situ* atomic force microscopy imaging, where t is time at elevated temperature $T - T_g \sim 12$ °C. Both methyl- and amine-functionalized nanosilica on poly(methyl methacrylate) and poly(methyl methacrylate)/methacrylic acid polymer surfaces were considered.

$A_{silica} = 8.63 \times 10^{-19}$ J[43]). Equation (6) is highly nonlinear, and accounts for van der Waals forces between the nanoparticle and polymer, which are confined by the viscous drag of polymer, as well as entropic effects due to particle incorporation into the polymer.[37] We were not able to experimentally determine η with high accuracy for these spin-coated PMMA and PMMA/MAA films of only 500 nm thickness. However, eqn (6) demonstrates how the relative differences in viscosity between these two polymers at the same elevated temperature can affect differences in velocity for the same functionalized nanosilica. For our nanoparticles of radius 10 nm and aforementioned magnitudes of A, the estimated initial sink-in velocity increases by ~60% (on the order of our experimentally observed differences for the two polymers) only if the polymer viscosity decreases by ~700%. It is thus unlikely that polymer viscosity is the predominant reason for the differences in nanoparticle sink-in velocity between these two polymers, as there exists only a two-fold variation in viscosity between these polymers of differing molecular weight.[44] (Note that eqn (6) could also be utilized as a different perspective on thermodynamic effects of nanoparticle functionalization, *via* variation in A_{silica} for constant η, though this is beyond the scope of the current study.) Previous contact mechanics-based models[45–50] have been proposed to account for polymer viscoelastic effects on particle sink-in rate. However, those models are valid only for particles that sink in to depths less than the particle radius.[46] In the present study at temperatures significantly above T_g, all nanoparticles moved to depths exceeding the particle radius – even for the least interactive polymer–particle system. Moreover, in the present study, the experiment temperature was about ~12 °C higher than T_g of the polymers, while previous models[45] are more applicable at or slightly below the T_g of polymers. Thus, it is unlikely that differences in polymer matrix viscosity are the predominant cause of differences in particle sink-in velocity among these systems. The second possibility, by which acrylic acid groups in the PMMA/MAA may interact with any remaining silanol groups on the methyl-functionalized nanosilica, cannot be quantified accurately on such small nanoparticles at this time. Both potential contributions to differential nanoparticle sink-in velocities remain intriguing areas for future study of tailored nanocomposites.

In light of subtle physical and chemical differences among polymer matrices discussed above, comparisons of sink-in velocity among particle–polymer systems are most fairly made when contrasting different surface functionalizations for a given polymer. Here we observed that initial sink-in velocity varied significantly with particle functionalization on either polymer, and was greater for amine functionalized nanosilica. This enhanced rate of interaction with respect to both the nanoparticle functionalization and the polymer matrix reactivity is consistent with the thermodynamic predictions, and further underscores the capacity to change both the speed and extent of interaction through independent variations of both particle and polymer chemistry.

3.4 Mechanical consequences at the macroscopic scale

To probe the influence of nanoscale particle–polymer interactions on the macroscale mechanical behavior, instrumented indentation and scratch tests were conducted on quasi-two-dimensional nanocomposite films. Briefly, these nanocomposite films were generated *via* heating of the strike method samples to sink-in the particles to equivalent heights that were less than the particle radius (see Experimental). Elastic moduli (E) obtained *via* indentation for PMMA-nanosilica and PMMA/MAA-nanosilica are shown in Table 1. The measured elastic modulus E for neat PMMA (no nanoparticles) is slightly lower than that of neat PMMA/MAA. However, as mentioned above, comparisons among these particle–polymer systems are most fairly made when comparing particles with different surface functionalization for a given polymer; the two matrices may differ in subtle ways related to molecular weight. Thus, as in the case of nanosilica sink-in analysis, we compared the elastic modulus E and scratch resistance among these samples as a function of nanosilica functionalization for each of the two polymers (PMMA *or* PMMA/MAA). Note that one shortcoming of our sample preparation methodology is that the initial particle density varies unpredictably among these materials, so the nanosilica "particle density" of these composites was quantified as the number of particles per μm^2.

As expected, E of both composites exceeded that of the pure ("neat") polymer, exhibiting greater stiffness by ~35% for PMMA (3.06 ± 0.08 GPa), and by 24% for PMMA/MAA (3.36 ± 0.11 GPa). More importantly, statistically significant differences in E of the composites were observed as a function of nanoparticle surface functionalization. In PMMA composites, the amine functionalized nanosilica resulted in a 14% increase in E of the composite (4.25 ± 0.32 GPa), as compared to methyl functionalized nanosilica (3.72 ± 0.28 GPa). This is particularly impressive because the measured particle density for the PMMA-amine functionalized nanosilica (5 ± 1 particle/μm^2) was 40% lower than that of methyl functionalized nanosilica (7 ± 1 particle/μm^2). Similar results were obtained for the PMMA/MAA-based nanocomposite films: amine functionalized nanosilica conferred a 7% increase in E for (4.31 ± 0.13 GPa) as compared methyl functionalized nanosilica (4.05 ± 0.10 GPa), notwithstanding a 50% lower particle density. In summary, although the particle density was not equivalent among all samples due to limitations of the strike method, we consistently observed a higher elastic modulus for composites containing nanoparticles that interacted more strongly with the polymer matrix.

Scratch resistance was quantified by measuring the removed volume per unit length in each scratch. Here, care was taken to achieve equivalent particle sink-in for all composites, since surface roughness also affects scratch resistance. Fig. 6a-b show AFM topography images and representative line traces over the scratches acquired on PMMA and the PMMA-nanosilica composite films. Figure 7 quantifies the volume of material removed per unit length for these samples. This comparison demonstrates a significant improvement of scratch resistance is conferred by the silica nanoparticles, even for the weaker particle–polymer interactions (methyl). In fact, the scratch volume removed on methyl functionalized nanosilica composites decreased by 32% compared to pure PMMA. Moreover, the scratch volume removed for amine functionalized nanosilica-PMMA composites was 43.5% less than that for pure PMMA and 17% less than that for methyl functionalized nanosilica-PMMA composites. Similar trends were observed for the

Table 1 Elastic modulus *E*, as measured *via* instrumented indentation (N = 20) for nanocomposite films prepared *via in situ* heating of the nanosilica–polymer samples prepared *via* the strike method described in the text. Comparison of neat poly(methyl methacrylate), or PMMA, and two PMMA-nanosilica composite films comprising either methyl (CH_3)- or amine (NH_2)-functionalized nanosilica; and separately of neat PMMA/methacrylic acid (MAA) and two PMMA/MAA-nanosilica composite films comprising either CH_3- or NH_2-functionalized nanosilica

	PMMA	PMMA-silica(–CH_3)	PMMA-silica(–NH_2)
E(GPa)	3.06±0.08	3.73±0.28	4.25±0.32
	PMMA/MAA	PMMA/MAA-silica(–CH_3)	PMMA/MAA-silica(–NH_2)
E(GPa)	3.36±0.11	4.05±0.15	4.31±0.13

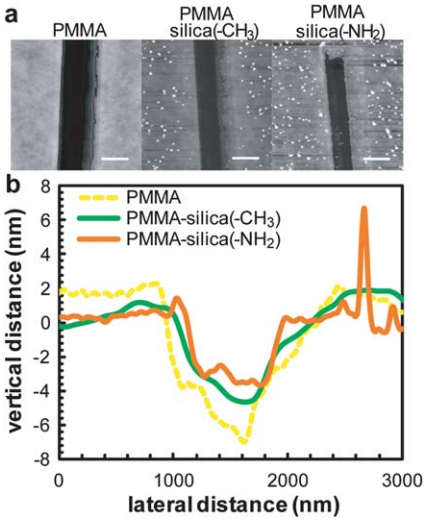

Fig. 6 (a) Atomic force microscopy topography images acquired in AC mode over imposed scratches in poly(methyl methacrylate), or PMMA, and two PMMA-nanosilica composite films comprising either methyl (CH_3)- or amine (NH_2)-functionalized nanosilica. (b) Representative topography line traces over these scratches enable qualitative comparison of scratch resistance, and volumetric assessment of removed material volume affords quantitative comparison among films. Scale bar = 1 μm.

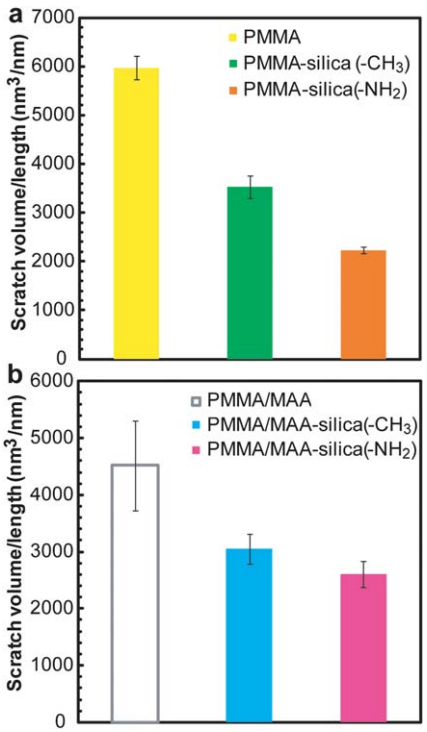

Fig. 7 Volume of material removed per unit scratch length for (a) neat PMMA, and two PMMA-nanosilica composite films comprising either methyl (CH_3)- or amine (NH_2)-functionalized nanosilica; and (b) neat PMMA/MAA and two PMMA/MAA-nanosilica composite films comprising either CH_3- or NH_2-functionalized nanosilica. N = at least 8 replicate analyzed scratches for each sample.

nanosilica-PMMA/MAA composites, although differences in scratch resistance as a function of nanoparticle surface functionalization were less pronounced and may also be attributable to the lower particle density for amine functionalized nanosilica. Thus, macroscopic scratch resistance clearly increased in accordance with increasing extent and speed of nanoparticle–polymer interactions.

4. Summary and outlook

In this study, we demonstrated that the interaction between polymers and nanoparticles can be tailored by modifying the surface chemistry of the silica as well as the reactivity of the polymer. Through *in situ* imaging of these nanoparticle–polymer interactions for well characterized nanosilica and PMMA systems, we confirmed that amine functionalized nanosilica interacts more strongly with the polymer than methyl functionalized nanosilica, both in terms of the extent and rate of interaction. This capacity to tune the nanoparticle–polymer interface has direct consequences for macroscopic mechanical properties of a nanocomposite, here resulting in significant increases in stiffness and scratch resistance for stronger nanoparticle–polymer interactions. For application toward bulk nanocomposites, we note that surface energetics affect both the particle–polymer interaction strength and the particle dispersion capacity within the matrix. However, in principle these goals of enhanced particle–polymer interactions and high particle dispersion are not mutually exclusive; our ongoing work includes extension of this approach to improve nanosilica dispersion in bulk PMMA. More generally, these *in situ* approaches provide direct and rapid analyses of the chemomechanical nanoparticle–polymer interactions that modulate composite properties.

Acknowledgements

We gratefully acknowledge funding from DuPont-MIT Alliance (DMA), as well as technical assistance from colleagues K. Lehman, S. Zane, and D. Brill.

References

1 Y. Li, J. Yu and Z.-X. Guo, *J. Appl. Polym. Sci.*, 2002, **84**, 827–834.

2 T. Ramanathan, A. A. Abdala, S. Stankovich, D. A. Dikin, M. Herrera-Alonso, R. D. Piner, D. H. Adamson, H. C. Schniepp, X. Chen, R. S. Ruoff, S. T. Nguyen, I. A. Aksay, R. K. Prud'homme and L. C. Brinson, *Nat. Nanotechnol.*, 2008, **3**, 327–331.
3 T. Zhou, X. Wang, M. Gu and D. Xiong, *Polym. J.*, 2009, **41**, 51–57.
4 J. S. Shelley, P. T. Mather and K. L. DeVries, *Polymer*, 2001, **42**, 5849–5858.
5 C. I. Park, O. O. Park, J. G. Lim and H. J. Kim, *Polymer*, 2002, **42**, 7465–7475.
6 C.-R. Tseng, J.-Y. Wu, H.-Y. Lee and F.-C. Chang, *J. Appl. Polym. Sci.*, 2002, **85**, 1370–1377.
7 E. A. Zaragoza-Contreras, C. A. Hernandez-Escobar, M. E. Mendoza-Duarte, S. G. Flores-Gallardo, R. Ibarra-Gomez and A. Marquez-Lucero, *Polym. J.*, 2009, **41**, 816–821.
8 C. Aymonier, D. Bortzmeyer, R. Thomann and R. Mulhaupt, *Chem. Mater.*, 2003, **15**, 4874–4878.
9 J. Jordan, K. I. Jacob, R. Tannenbaum, M. A. Sharaf and I. Jasiuk, *Mater. Sci. Eng., A*, 2005, **393**, 1–11.
10 B. J. Ash, R. W. Siegel and L. S. Schadler, *Macromolecules*, 2004, **37**, 1358–1369.
11 B. J. Ash, R. W. Siegel and L. S. Schadler, *Journal of Polymer Science*, 2004, **42**, 4371–4383.
12 P. H. T. Vollenberg and D. Heikens, *Polymer*, 1989, **30**, 1656–1662.
13 K. H. Wang, I. J. Chung, M. C. Jang, J. K. Keum and H. H. Soong, *Macromolecules*, 2002, **35**, 5529–5535.
14 Y. Zhang, S. Ge, B. Tang, M. H. Rafailovich, J. C. Sokolov, D. G. Peiffer, Z. Li, A. J. Dias, K. O. McElrath, S. K. Satija, M. Y. Lin and D. Nguyen, *Langmuir*, 2001, **17**, 4437–4442.
15 F. Yang and G. L. Nelson, *J. Appl. Polym. Sci.*, 2004, **91**, 3844–3850.
16 Y.-L. Liu, C.-Y. Hsu and K.-Y. Hse, *Polymer*, 2005, **46**, 1851–1856.
17 Y.-Y. Yu, C.-Y. Chen and W.-C. Chen, *Polymer*, 2003, **44**, 593–601.
18 T. Kashiwagi, A. B. Morgan, J. M. Antonucci, M. R. VanLandingham, R.H.H. Jr., W. H. Awad and J. R. Shields, *J. Appl. Polym. Sci.*, 2003, **89**, 2072–2078.
19 J. S. Meth and S. R. Lustig, *Polymer*, 2010, **51**, 4259–4266.
20 V. M. Litvinov and P. A. M. Steeman, *Macromolecules*, 1999, **32**, 8476–8490.
21 W. Hergeth, U. Steinau, H. Bittrich, G. Simon and K. Schmutzler, *Polymer*, 1989, **30**, 254–258.
22 E. Tadd, A. Zeno, M. Zubris, N. Dan and R. Tannenbaum, *Macromolecules*, 2003, **36**, 6497–6502.
23 F. W. Starr and S. C. Glotzer, in *Materials Research Society Symposium Proceedings*, Materials Research Society, Warrendale, OH, 2001.
24 C. L. Wu, M. Q. Zhang, M. Z. Rong and K. Friedrich, *Compos. Sci. Technol.*, 2002, **62**, 1327–1340.
25 L. T. Zhuravlev, *Langmuir*, 1987, **3**, 316–318.
26 A. W. Adamson and A. P. Gast, *Physical Chemistry of Surfaces*, John Wiley & Sons, Inc., New York, 1997.
27 D. R. Lide, *CRC handbook of chemistry and physics: a ready-reference book of chemical and physics*, CRC Press LLC, Boca Raton, Florida, 2004.
28 G. J. Kovacs and P. S. Vincett, *J. Colloid Interface Sci.*, 1982, **90**, 335–351.
29 G. J. Kovacs and P. S. Vincett, *Thin Solid Films*, 1984, **111**, 65–81.
30 F. M. Fowkes, *J. Phys. Chem.*, 1962, **66**, 382.
31 G. Constantinides, K. S. R. Chandran, F.-J. Ulm and K.-J. VanVliet, *Mater. Sci. Eng., A*, 2006, **430**, 189–202.
32 J. Brandrup, E. H. Immergut, E. A. Gruike, A. Abe and D. R. Block, *Polymer Handbook* (4th edition), John Wiley & Sons, 2005.
33 Y. Sun, Z. Zhang and C. P. Wong, *J. Colloid Interface Sci.*, 2005, **292**, 436–444.
34 Y. Sun, Ph.D. Thesis, Georgia Institute of Technology, 2006, p. 216.
35 J. Erichsen, J. Kanzow, U. Schrmann, K. Dolgner, K. Gnther-Schade, T. Strunskus, V. Zaporojtchenko and F. Faupel, *Macromolecules*, 2004, **37**, 1831–1838.
36 D. S. Rimai, D. M. Schaefer, R. C. Bowen and D. J. Quesnel, *Langmuir*, 2002, **18**, 4592–4597.
37 R. D. Deshmukh and R. J. Composto, *Langmuir*, 2007, **23**, 13169–13173.
38 S.-J. Park and J.-S. Kim, *J. Colloid Interface Sci.*, 2000, **232**, 311–316.
39 R. Asthana and N. Sobezak, in *Journal of Metals*, 2000.
40 S.-J. Park, K.-S. Cho and S.-K. Ryu, *Carbon*, 2003, **41**, 1437–1442.
41 P. C. Hiemenz and R. Rajagopalan, *Principles of colloid and surface chemistry*, Dekker, New York, 1997.
42 N. G. Semaltianos, *Microelectron. J.*, 2007, **38**, 754–761.
43 A. Silva, R. Brazda, J. Zegzulka, R. Dvorsky and J. Lunacek, *Journal of Scientific Conference Proceedings*, 2010, **2**, 45–48.
44 J. J. Kirkland and S. W. Rementer, *Anal. Chem.*, 1992, **64**, 904–913.
45 S. A. Hutcheson and G. B. McKenna, *Phys. Rev. Lett.*, 2005, **94**, 076103.
46 E. H. Lee and J. R. M. Radok, *Journal of Applied Mechanics*, 1960, **27**, 438–444.
47 T. C. T. Ting, *Journal of Applied Mechanics*, 1966, **33**, 845–854.
48 Z. Fakhraai and J. A. Forrest, *Science*, 2008, **319**, 600–604.
49 D. Qi, Z. Fakhraai and J. A. Forrest, *Phys. Rev. Lett.*, 2008, **101**, 096101.
50 J. H. Teichroeb and J. A. Forrest, *Phys. Rev. Lett.*, 2003, **91**, 016104.
51 M. Qu, F. Deng, S. Kalkhoran, A. Gouldstone, A. Robisson and K. J. Van Vliet, *Soft Matter*, 2011, **7**, 1066–1077.

